Regional contrasts in dust emission responses to climate

Charles S. Zender and Eun Young Kwon
Department of Earth System Science, University of California, Irvine, California, USA

Received 9 October 2004; revised 23 February 2005; accepted 28 March 2005; published 7 July 2005.

[1] Time-series analysis of Earth's major dust source regions reveals common traits in responses of wind erosion to climate anomalies. Lag cross-correlations of monthly mean aerosol optical depth, precipitation, vegetation, and wind speed are examined from 1979–1993. The response to monthly climate anomalies can differ greatly from the response to seasonal mean climate. The signs, magnitudes, and lags of highly significant ($p < 0.01$) correlations show that 14 important mineral dust source areas characterized by Prospero et al. (2002) fall into four response categories. Each category represents distinct mechanisms by which climate anomalies influence subsequent atmospheric dust loading on seasonal to interannual timescales. In most regions, precipitation and vegetation together strongly constrain dust anomalies on multiple timescales. In these regions, dry anomalies increase, and wet anomalies reduce, dust emission. Interestingly, in many other regions the contrary is true: Dust and precipitation anomalies correlate positively, consistent with sediment-supply factors. The response timescales are consistent with loss of surface crusts (less than 1 month) and with alluvial transport and dessication (interannual lags). Supply-limited dust emission appears more prevalent than previously thought and is not accounted for in models. Reproducing these wind erodibility responses in models may help remediate underprediction of observed seasonal to interannual dust variability.

Citation: Zender, C. S., and E. Y. Kwon (2005), Regional contrasts in dust emission responses to climate, *J. Geophys. Res.*, *110*, D13201, doi:10.1029/2004JD005501.

1. Introduction

[2] Atmospheric mineral dust plays important roles in climate. In addition to direct radiative forcing [*Tegen et al.*, 1997], dust participates in indirect climate forcing through its role as a cloud-condensation nucleus [e.g., *Wurzler et al.*, 2000] and potential atmospheric CO_2 regulator via biospheric nutrient delivery [*Fung et al.*, 2000]. Conversely, climate conditions control dust emission, transport, and deposition [*Prospero and Nees*, 1986], forming a feedback loop. Hence understanding desert wind erodibility responses to climate change can help us interpret the many climate changes recorded in aeolian sediments. Here we identify commonalities in observed responses of Earth's dustiest regions to climate anomalies. Reproducing these responses in models is an important test of modeling skill at predicting future dust loading and related climate change.

[3] Building upon earlier studies [e.g., *Pye*, 1987; *Goudie et al.*, 1999], researchers have elucidated multiple climate controls on dust in the past 2 decades. Periods of high dust concentration in Barbados correspond to North African drought up to 2 or 3 years prior, and are most highly correlated with previous year rainfall [*Prospero and Nees*, 1986; *Prospero and Lamb*, 2003]. Drought reduces vegetation density and extent and increases soil vulnerability to wind erosion [*Gillette and Passi*, 1988; *Nicholson et al.*, 1998]. Rain and ground water help form soil crusts that can reduce wind erodibility by an order of magnitude or more until wind or other mechanisms (including anthropogenic) disrupt the crusts [*Gillette and Passi*, 1988; *Gill*, 1996; *Gillette et al.*, 2001]. That precipitation can enhance wind erodibility is well documented though lesser known. In some regions, heavy rain provides fine material through deposition of flood-transported sediments [*McTainsh et al.*, 1999, 2002] which increases erodibility during subsequent dry periods.

[4] Local topography, regional geomorphology, and surface hydrology also influence local erodibility and improve dust hindcasts in global models [*Engelstaedter et al.*, 2003; *Zender et al.*, 2003b]. Aeolian erodibility is the capacity of a soil to erode due to meteorological forcing (e.g., wind stress). *Zender et al.*, [2003a, equation (17)] and *Zender et al.* [2003b, equation (1)] quantify wind erodibility S as the ratio of actual vertical dust mass flux to the mass flux mobilized from an idealized surface in the absence of regional geographic influences. This paper addresses the influences of prior climate conditions that promote subsequent dust emission. An erodibility anomaly in this context is a temporal change in the capacity of the soil to erode. Our results below strongly suggest that dust forecasts should represent the effects of temporal changes in sediment supply (e.g., soil crusting,

0148-0227/05/2004JD005501$09.00

alluvial recharge) heretofore neglected in global wind-erosion models.

2. Methods

[5] Isolated dust events occur for manifold reasons dependent on instantaneous micro-meteorology and surface conditions. These events are best examined with in situ data and observations. Satellite observations, however, are well suited to studying the relation between climate and dust loading in disparate source regions on seasonal-to-interannual timescales [*Prospero et al.*, 2002; *Washington et al.*, 2003]. *Torres et al.* [2002] estimated dust Aerosol Optical Depth (AOD) from Total Ozone Mapping Spectrometer (TOMS) measurements. TOMS AOD typically agrees with ground-based observations within 30% [*Torres et al.*, 2002] and is an adequate proxy for dust emissions in source regions [*Prospero et al.*, 2002]. The AOD retrieval worsens for highly absorptive aerosol, and for aerosol contained in shallow boundary layers [*Mahowald and Dufresne*, 2004]. TOMS AOD data spatial resolution is $1^\circ \times 1^\circ$. Time series occur in two distinct periods: January 1979 to April 1993, and August 1996 to 2000. For consistency in temporal variation, we use Nimbus7 data only, collected from January 1979 to April 1993. AOD retrievals in remote dust source areas are less contaminated by carbonaceous aerosol because of their distance from industry and biomass burning. We omit some regions, such as the western Sahel, where discriminating dust from carbonaceous aerosol plumes is problematic.

[6] Climate-related dust-emission controls monitored from space include precipitation and vegetation. For precipitation data we use the monthly Global Precipitation Climatology Project (GPCP) Version 2 Combined Precipitation Dataset. GPCP data were produced by merging infrared and microwave satellite data with rain gauge data [*Huffman et al.*, 1997] beginning in January 1979. The spatial resolution is $2.5^\circ \times 2.5^\circ$. Hence TOMS and GPCP data provide spatially and temporally consistent information regarding mineral dust loading and rainfall amount.

[7] Normalized Difference Vegetation Index (NDVI) is correlated with surface-vegetation cover, a primary dust-emission constraint [*Nicholson et al.*, 1998]. However, two-channel NDVI has many limitations as a proxy for vegetation cover in arid regions. These limitations include insensitivity to non-photosynthetic (NPV) vegetation, open canopies, and low spectral contrast [*Okin et al.*, 2001]. We use NDVI retrieved from Advanced Very High Resolution Radiometer (AVHRR) measurements with one-degree resolution from January 1981 to September 1994. For surface wind velocity, we use National Centers Environmental Prediction (NCEP) surface re-analyses [*Kalnay*, 1996].

[8] The data processing procedure is as follows. First, values within a specific source region are averaged for each month and each data set from January 1979 to April 1993. As an example, Figure 1 shows time series for the eastern Sahel, defined as 10°N–15°N, 10°W–20°E (we omit the western Sahel to reduce AOD cross-contamination from biomass burning plumes). Minimal and maximal rainfall occurs in 1984 and 1988, respectively. Anti-correlated dust responses appear approximately 9 months later. Second, we remove the seasonal cycles by subtracting fitted sinusoidal functions from the original data. The seasonal cycles subtracted from the analyses appear as dashed lines in Figure 1. Third, we remove the effects of auto-correlation from the monthly anomalies. The number of months p at which the anomaly time series are significantly self-correlated, and the auto-correlation contribution to the anomaly time series, are determined using an Auto-Regressive model of order p, denoted AR(p) [*Chatfield*, 2004]. Rainfall and AOD have significant AR(1) and AR(2) processes, respectively, which we remove.

[9] We examined lags as long as 60 months for statistically robust cross-correlations r (the total data length is $N = 168$ months). Figure 2 (left) shows the cross correlation for the eastern Sahel region. The dashed lines demarcate outliers above the 99% significance level, determined by dividing 3 by the square root of the total number of data points ($N = 168$) [*Chatfield*, 2004]. The only highly significant correlation between dust loading and prior precipitation over the eastern Sahel (see Figure 1) occurs with a 9-month lag. The Tarim Basin, in contrast to the eastern Sahel, exhibits no significant relation between monthly dust loading and prior rainfall (Figure 2, right).

[10] The normalized seasonal cycle (seasonal cycle less the climatological mean, divided by the monthly standard deviation) of dust loading and three climate controls in four source regions shows that the seasonal peak in dust load is usually quite distinct (Figure 3). Assuming that most dust mobilization is natural (not anthropogenic), the seasonal peak coincides with the optimal climate state for wind eroding a region's surfaces. Viewed as a multiple constraint problem, peak emission occurs when the product of multiple dust-emission constraints (wind, vegetation, soil moisture, sediment availability, etc.) is minimal. However, the seasonal emission peak teaches us little about the relative roles of individual factors. Our analysis procedure helps identify the climatic precursors of dust anomalies. The identified factors are the likeliest causes of monthly deviations from the mean seasonal cycle. For this reason we call these factors the primary or "rate-limiting" dust-emission controls.

3. Results

[11] The procedure described above produces a matrix (Table 1) of highly significant ($p < 0.01$) erodibility responses to climate in many of Earth's most significant dust-emitting regions as detected from space. *Prospero et al.* [2002] and *Washington et al.* [2003] describe the geographic features, climatology, geomorphology, and soil characteristics, and the extent, intensity, and seasonality of dust emissions in these regions. The second column of Table 1 contains the cross correlations of precipitation P and AOD τ. The cross-correlation sign and lag differ regionally. NDVI and wind speed data are processed in the same manner as precipitation and AOD. Columns three to six contain cross correlations between precipitation and NDVI, between NDVI and dust loading, precipitation and wind, and wind and dust loading. Of the 14 source regions, monthly dust anomalies are directly and significantly related to precipitation in 12, to vegetation in eight, and to wind speed in two. Hence precipitation anomalies appear to be the best climate predictor of monthly dust anomalies.

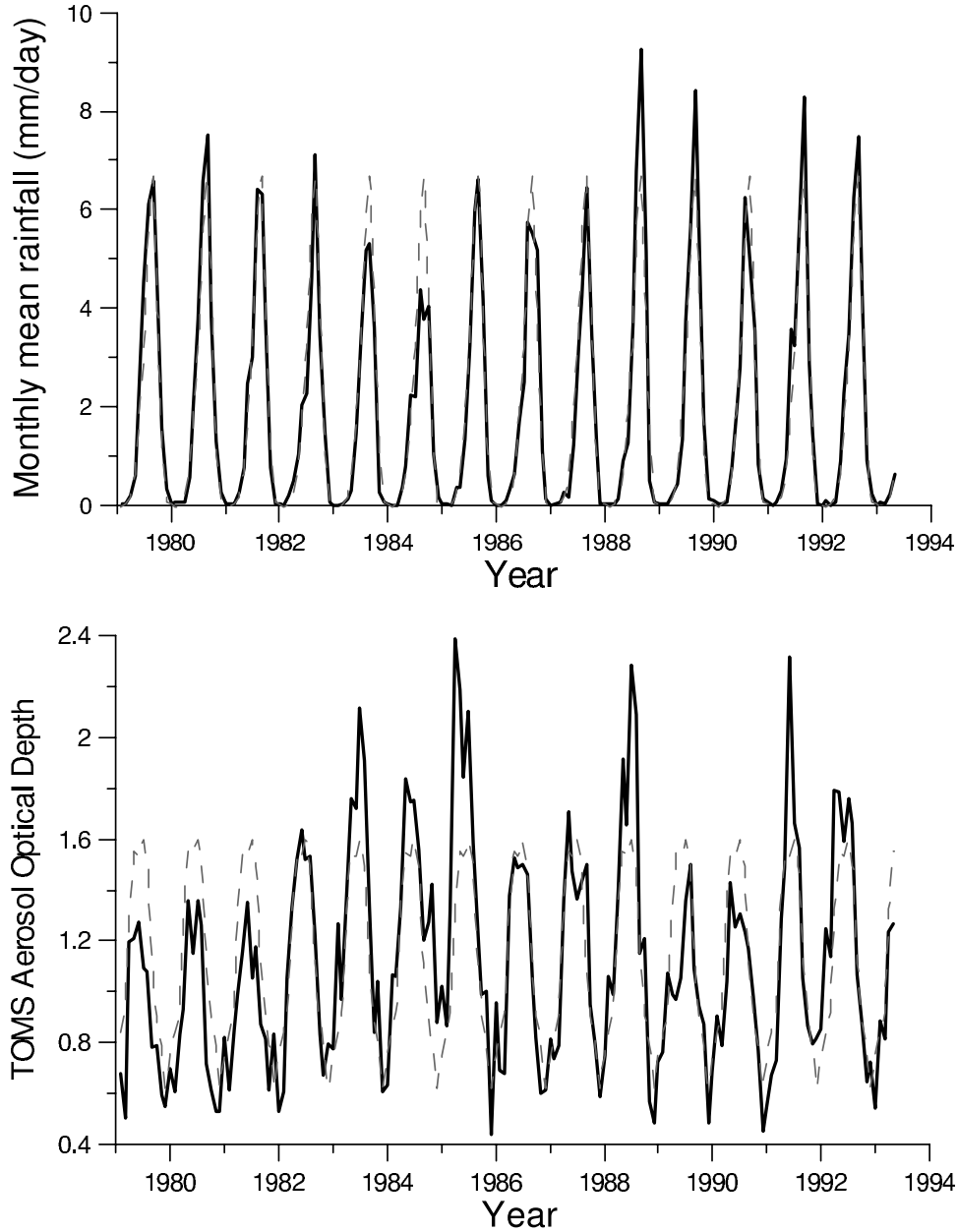

Figure 1. Monthly mean satellite-derived (top) GPCP precipitation [mm d^{-1}] and (bottom) TOMS dust Aerosol Optical Depth over the Eastern Sahel from January 1979 through April 1993. Solid lines are original data, and dashed lines are fitted seasonal cycles.

[12] The highly significant correlations between climate processes and the AOD proxy for dust emission in Table 1 may indicate causal relations. The regions we examined fell into one of four categories of wind-erosion response to climate. The chief determinant of each category is the sign and lag of the dust response to precipitation anomaly. Categories I and II comprise regions characterized by negative correlations between precipitation and dust loading. Negative P, τ correlations indicate that drought causes anomalously high dust loading and/or that excess rainfall is correlated with anomalously low dust concentration. Categories III and IV comprise regions where precipitation and dust are positively correlated. Positive P, τ correlations indicate either that drought suppresses erodibility or, more likely, that excess rainfall enhances dust deflation. The precipitation sign and lag, together with the behavior of NDVI and wind speed, help to further elucidate the physical mechanisms underlying these categories.

[13] Vegetation and precipitation time series are measured independently, so we treat them mathematically as independent controls on dust emission. However, precipitation controls vegetation in arid regions on monthly timescales [e.g., *Peters and Eve*, 1995; *Weiss et al.*, 2004]. Hence the vegetation influence on dust is inextricably linked to precipitation, as Table 1 indicates.

[14] Highly significant negative cross correlations between precipitation and African dust have been shown in

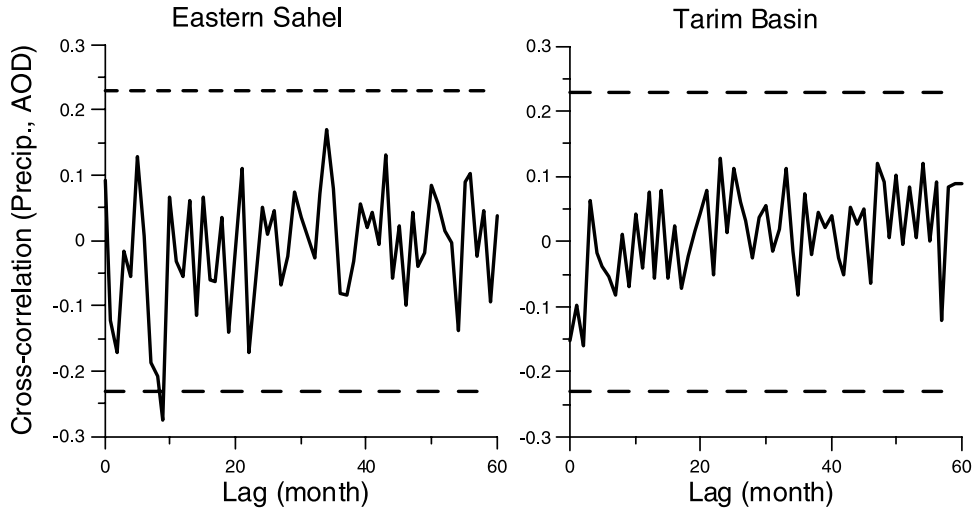

Figure 2. Lag cross-correlation of autoregression-corrected monthly mean seasonal precipitation and dust anomalies over the (left) Eastern Sahel and (right) Tarim Basin. Confidence levels with $p < 0.01$ are at ±0.23, shown as dashed lines.

previous studies [e.g., *Prospero and Nees*, 1986; *Nicholson et al.*, 1998; *Mahowald et al.*, 2003a]. Not surprisingly, the anti-correlation between precipitation and dust emission is widespread among Earth's dustiest regions (Table 1). In many regions, anomalous rainfall triggers a consistent NDVI response within 1 month. In six of these regions, the NDVI anomaly significantly influences dust in the same or the subsequent month. We classify these six regions as Category I; they include the eastern Sahel and Bodele Depression in Africa, the western United States, Lake Eyre basin in Australia, Botswana, and the Thar Desert in India. The immediate dust response to precipitation in Category I regions is consistent with surface soil moisture increasing soil cohesion and wind friction threshold speeds [*Fécan et al.*, 1999]. However, the vegetation constraint is often stronger, and usually more immediate, than the precipitation constraint.

[15] The vegetative constraint in Category I regions ranges from explaining slightly less to slightly more AOD variability than precipitation itself (Table 1). The wind erodibility responds on two timescales: immediate (0–1 month) and 9–10 months. The immediate vegetation constraint is consistent with quick growth of opportunistic arid vegetation during wet periods [*Okin et al.*, 2001]. A 9–10 month lag may indicate changes in dust emissions during the next dry season following an anomalously wet season, as in Figure 3a. This association is consistent with non-photosynthetic vegetation (NPV) remaining months after the initial greenness burst detected in the NDVI anomaly [*Okin et al.*, 2001]. *Nicholson et al.* [1998] describe how Sahelian vegetation advances toward or retreats from the Sahara desert depending on the annual rainfall amount. Hence it appears that both vegetation extent and density mediate wind erodibility in Category I regions. Our results show that precipitation-induced vegetation anomalies alter wind erodibility on monthly, and possibly shorter, timescales.

[16] Vegetation anomalies significantly influence dust emissions anomalies in the Gobi Desert 2 months later (Table 1). However, there is no detectable link between Gobi dust and rainfall anomalies. TOMS aerosol retrievals also fail to detect known Gobi dust sources, possibly because of temporal sampling and cloud-screening issues associated with the infrequent springtime frontal systems thought to generate much of the Gobi dust [*Prospero et al.*, 2002; *Washington et al.*, 2003]. The relatively low quality of TOMS retrievals in the Gobi may help explain the absence of a detectable relation between dust and precipitation here. Although the fit is not ideal, we classify the Gobi Desert as Category I based on the vegetation influence alone.

[17] Two regions, China's loess plateau and the Great Salt Lake, have instantaneous (0 month) negative cross correlations between precipitation and dust loading. Unlike Category I regions, these two regions exhibit no detectable highly significant vegetation constraints. We classify as Category II these regions whose dust response is anti-correlated with precipitation and uncorrelated with NDVI.

[18] We emphasize that the entire Chinese loess plateau comprises a wide range in climate setting and vegetation and that our analyses apply only to the average of these dust influences over the selected region. As mentioned above, our NDVI data do not detect most non-photosynthetic vegetation, which can be a significant dust-emission constraint in arid regions [*Okin et al.*, 2001]. Seasonal winds and dust peak together in the Chinese loess plateau (Figure 3d), so it is also noteworthy that there is no significant relation between the wind and dust anomalies.

[19] Five of the 14 regions examined have highly significant positive cross correlations between precipitation and dust loading anomalies. The positive correlation implies that precipitation is conducive to dust emissions in these regions, which comprise Categories III and IV. Unlike Categories I and II, the dominant constraint on monthly anomalies on seasonal to interannual timescales in these regions may be supply limitation, i.e., availability of loose sediment vulnerable to saltation and sandblasting [*Gillette*, 1978; *Gomes et al.*, 1990].

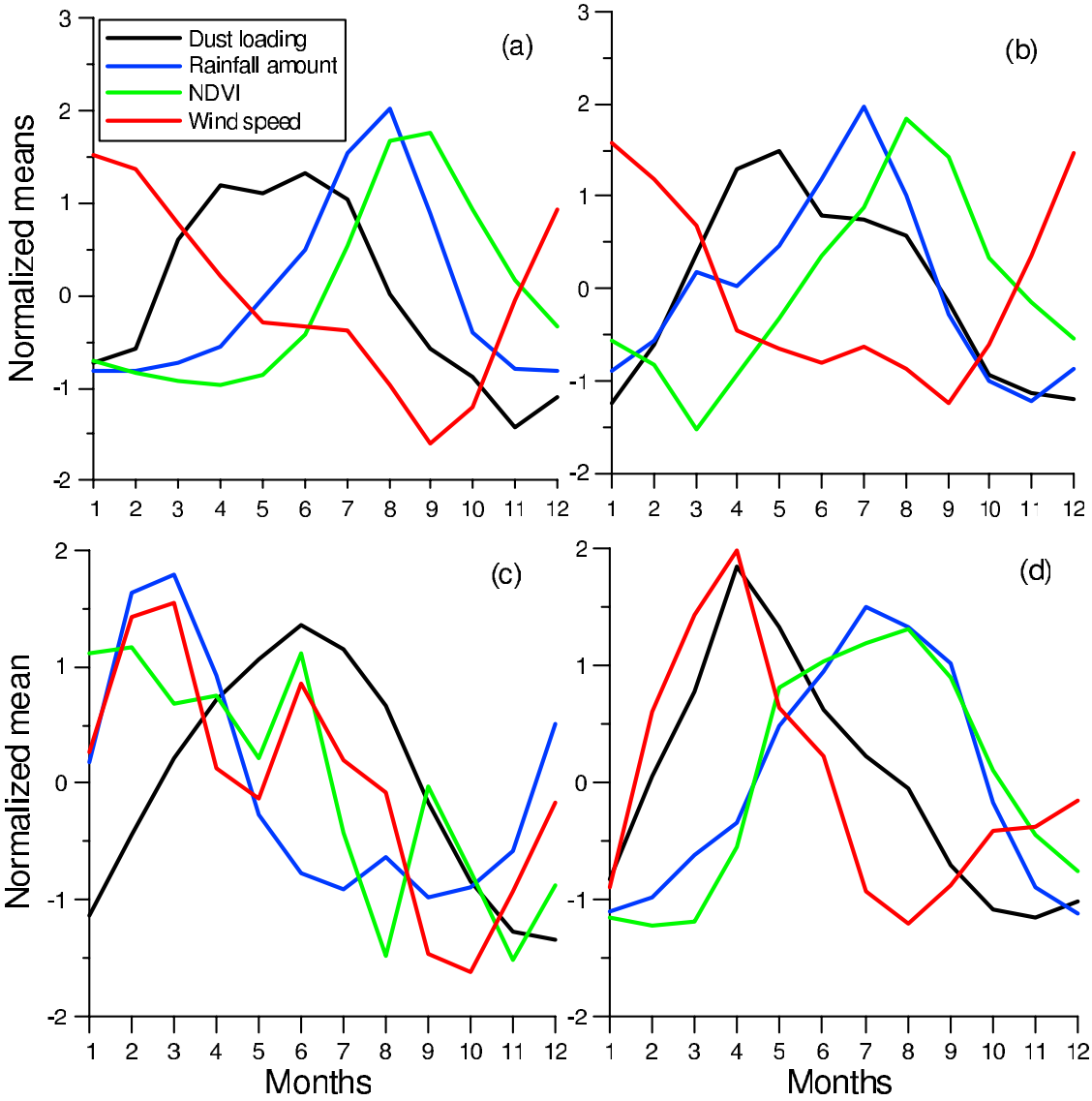

Figure 3. Normalized seasonal cycle of atmospheric dust (black), precipitation (blue), NDVI (green), and surface wind speed (red) over (a) Eastern Sahel, (b) Tarim Basin, (c) Saudi Arabia, and (d) Chinese loess plateau.

[20] A prominent feature of two of these regions, the Zone of Chotts in North Africa and the Tigris-Euphrates Basin, is that the P, τ cross-correlation lags are interannual: 44 and 14 months, respectively. There is no P, τ cross-correlation lag in the other three regions: Saudi Arabia, Oman, and the Thar Desert. The interannual dust-emission response is compatible with intermittent fluvial delivery of fine-grained sediment to areas of dust emission. Alluvial surfaces are vulnerable to deflation after dessication in subsequent dry periods [*Lima et al.*, 1992; *Gill*, 1996; *Prospero et al.*, 2002]. These results are consistent with *Mahowald et al.* [2003a], who showed direct but inconclusive satellite evidence for increased dust loading after the drying of flooded ephemeral lakes in the Zone of Chotts, and with in situ observations of precipitation and dust emissions from clay pans in eastern Australia [*McTainsh et al.*, 1999, 2002]. We classify as Category III those regions where monthly dust anomalies are dominated by an interannual response to precipitation.

[21] In three of the remaining regions (Saudi Arabia, Oman, and the Thar Desert) the highly significant positive correlations between precipitation and dust anomalies are lag-free, occurring in the same month. Hence our Category IV encompasses source regions where evidence points to faster processes such as disruption of surface crusts rather than slower processes like alluvial recharge as the supply limitation constraints. Saudi Arabia stands out in Figure 3 because its seasonal dust maximum occurs soon after (rather than before) the rainy season, coincident with the summer monsoon. The same phasing occurs in Oman (not shown).

[22] In these evaporative tidal flats and wadis [*Prospero et al.*, 2002], seasonal winds and rains peak in winter. Ephemeral crusts formed during anomalously wet winters would therefore be vulnerable to wind disruption. Previous

Table 1. Erodibility Responses of Major Dust Source Regions[a]

Region	P, τ	P, N	N, τ	P, U	U, τ	Erodibility Category Assigned
Eastern Sahel, 10°N–15°N, 10°W–20°E	−0.27(9)	+0.33(1)	−0.31(0)			I
Bodele Depression, 15°N–20°N, 10°E–20°E	−0.28(9)	+0.26(9)	−0.31(0)			I
Western United States, 25°N–35°N, 110°W–100°W	−0.22(0)	+0.47(1)	−0.35(0)			I
Lake Eyre Basin, 30°S–25°S, 136°E–145°E	−0.36(1)	+0.61(1)	−0.29(1)			I
Botswana, 25°S–20°S, 20°E–30°E	−0.39(1), −0.23(0)	+0.56(2), +0.31(0)	−0.28(9)			I
Gobi Desert, 42.5°N–45°N, 105°E–110°E			−0.28(2)			I
Chinese Loess Plateau, 32.5°N–37.5°N, 105°E–110°E	−0.27(0)					II
Great Salt Lake, 40°N–42.5°N, 115°W–112.5°W	−0.37(0)	−0.27(0)		+0.26(0)		II
Zone of Chotts, 32.5°N–35°N, 5°E–10°E	+0.21(44)	+0.42(26)		+0.26(0)		III
Tigris/Euphrates, 27.5°N–32.5°N, 45°E–57.5°E	+0.21(14)	−0.26(8)				III
Saudi Arabia, 20°N–25°N, 47.5°E–52.5°E	+0.36(0)	−0.27(0)				IV
Oman, 17.5°N–20°N, 52.5–57.5°E	+0.40(0)					IV
Tarim Basin, 35°N–40°N, 75°E–90°E			+0.28(21)		+0.23(0), −0.24(2)	IV
Thar Desert, 25°N–30°N, 70–75°E	+0.25(0), −0.24(1), −0.21(2)	+0.57(1)	−0.3(0), −0.33(10)	−0.35(0)	+0.3(1)	I, IV

[a]Highly significant ($p < 0.01$) cross correlations r between autoregression-corrected erodibility indicators (dust AOD τ) and climate constraints (precipitation P, NDVI N, and wind speed U) from 1979–1994. Lag in months of indicated cross-correlation is shown in parentheses. Sources are as follows. Dust source regions identified by *Prospero et al.* [2002] and subsequent analyses of *Torres et al.* [2002] data.

studies clearly link the summer dusty season to summer monsoon winds [*Prospero et al.*, 2002; *Washington et al.*, 2003].

[23] It is instructive to contrast the eastern Sahel and Tarim Basin. These regions have nearly identical normalized seasonal cycles (Figure 3a and 3b) and dust peaks 9 months after precipitation. This seasonal cycle phasing probably explains the 9-month lag between Sahelian precipitation and dust anomalies apparent in Figure 2 (left). However, dust anomalies in the Tarim Basin are linked to wind anomalies (Table 1), not to precipitation (Figure 2, right). Hence the emissions mechanisms underlying monthly dust anomalies may differ greatly from the mechanisms that dominate seasonal emissions.

[24] The seasonal cycles of dust and wind in the Tarim Basin are highly correlated (Figure 3b). The most active dust regions in the Tarim Basin include many saline playas receiving significant drainage from spring snow melt [*Prospero et al.*, 2002]. We tentatively label the Tarim Basin as a Category IV region where anomalous winds disturb surface crusts formed by drainage or efflorescence [*Gill*, 1996] rather than precipitation. *Gillette et al.* [2001] documented this phenomena at Owens Dry Lake, where positive wind anomalies can dramatically increase dust production by disrupting sediment-limiting crusts.

[25] The Thar Desert region, including Rajasthan in India and the Indus drainage in Pakistan, fits criteria for Categories I and IV. Interpretation of dust emission anomalies in this region is difficult because the region contains anthropogenic activity [*Gill*, 1996], complex drainage systems [*Washington et al.*, 2003], and wind-deflated desert areas with limited silt vulnerable to sandblasting [*Prospero et al.*, 2002]. Table 2 summarizes our analysis of the four categories of erodibility response to climate.

4. Discussion and Conclusions

[26] We used monthly satellite-derived and blended time series to examine the relations of precipitation, vegetation, and wind-speed anomalies to subsequent mineral dust anomalies. Fourteen of Earth's dustiest regions display highly significant links between monthly climate and atmospheric dust anomalies on seasonal to interannual timescales. Some regions with very similar seasonal cycles and phasing of climate and dust load display quite different dust emission responses to climate anomalies. Four distinct wind-erodibility categories occur in these source regions. Each category represents distinct mechanisms by which climate influences subsequent atmospheric dust loading. In six regions, precipitation and vegetation together strongly constrain dust anomalies on multiple timescales. In two regions, dust responds immediately to precipitation anomalies, with no detectable vegetation constraint. More work is needed to assess the potential influence of non-photosynthetic vegetation in these regions.

Table 2. Erodibility Categories of Major Dust Source Regions

Category	Response[a]	Description	Regions
I	$P \downarrow \tau$, $P \uparrow N$, $N \downarrow \tau$	strong moisture and vegetation constraints, multiple timescales	Eastern Sahel, Bodele Depression, western United States, Lake Eyre, Botswana, (Gobi Desert)
II	$P \downarrow \tau$	strong moisture constraints, immediate response	Chinese Loess Plateau, Great Salt Lake
III	$P \uparrow \tau$	supply-limited, interannual alluvial recharge?	zone of Chotts, Tigris/Euphrates
IV	$P \uparrow \tau$	supply-limited, surface crust formation/loss	Saudi Arabia, Oman, Tarim Basin, Thar Desert

[a]Positive and negative correlations indicated by arrows pointing upward and downward, respectively.

[27] In six regions, dust and precipitation anomalies correlate positively, consistent with sediment-supply constraints. The response timescales are consistent with formation and loss of surface crusts (less than 1 month) and with alluvial transport and dessication (interannual lags). Some global models implicitly represent time-mean sediment supply [*Ginoux et al.*, 2001; *Tegen et al.*, 2002; *Zender et al.*, 2003b], but none explicitly represent time-varying sediment supply constraints such as alluvial recharge and formation and destruction of surface crusts. This condition may help explain why models underpredict high interannual dust variability in many regions [*Cakmur et al.*, 2001; *Mahowald et al.*, 2003b].

[28] Our method provides a quantitative procedure for classifying source regions into a conceptual framework of erodibility conditions that dominate dust anomalies on monthly timescales. These conditions are considered the dominant or ''rate-limiting'' factors on monthly dust variability; they do not necessarily explain seasonal or climatological mean dust patterns. Source-limitation factors such as fluvial sediment supply as well as surface crusting and efflorescence appear to be more prevalent than previously recognized. We recommend coordinated observational and modeling studies to increase understanding and improve model parameterizations of supply limitations. This approach will contribute to the goal of improving models for predicting dust loading and related climate change.

[29] **Acknowledgments.** This research was supported by NASA NAG 510546 and by NSF ATM 0214430 and OCE 0221516. We thank F. Primeau for detailed comments and discussions on data analysis, and two anonymous reviewers who improved the presentation of the results.

References

Cakmur, R. V., R. Miller, and I. Tegen (2001), A comparison of seasonal and interannual variability of soil dust aerosols over the Atlantic Ocean as inferred by the TOMS AI and AVHRR AOT retrievals, *J. Geophys. Res.*, *106*, 18,287–18,303.

Chatfield, C. (2004), *The Analysis of Time Series*, sixth ed., CRC, Boca Raton, Fla.

Engelstaedter, S., K. Kohfeld, I. Tegen, and S. Harrison (2003), The control of dust emissions by vegetation and topographic depressions: An evaluation using dust storm frequency data, *Geophys. Res. Lett.*, *30*(6), 1294, doi:10.1029/2002GL016471.

Fécan, F., B. Marticorena, and G. Bergametti (1999), Parameterization of the increase of the aeolian erosion threshold wind friction velocity due to soil moisture for arid and semi-arid areas, *Ann. Geophys.*, *17*, 149–157.

Fung, I. Y., S. K. Meyn, I. Tegen, S. C. Doney, J. G. John, and J. K. B. Bishop (2000), Iron supply and demand in the upper ocean, *Global Biogeochem. Cycles*, *14*, 281–296.

Gill, T. E. (1996), Eolian sediments generated by anthropogenic disturbance of playas: Human impacts on the geomorphic system and geomorphic impacts on the human system, *Geomorphology*, *17*, 207–228.

Gillette, D. (1978), A wind tunnel simulation of the erosion of soil: Effect of soil texture, sandblasting, wind speed, and soil consolidation on dust production, *Atmos. Environ.*, *12*, 1735–1743.

Gillette, D. A., and R. Passi (1988), Modeling dust emission caused by wind erosion, *J. Geophys. Res.*, *93*, 14,233–14,242.

Gillette, D. A., T. C. Niemeyer, and P. J. Helm (2001), Supply-limited horizontal sand drift at an ephemerally crusted, unvegetated saline playa, *J. Geophys. Res.*, *106*, 18,085–18,098.

Ginoux, P., M. Chin, I. Tegen, J. Prospero, B. Holben, O. Dubovik, and S.-J. Lin (2001), Sources and distributions of dust aerosols simulated with the GOCART model, *J. Geophys. Res.*, *106*, 20,555–20,273.

Gomes, L., G. Bergametti, G. Coudé-Gaussen, and P. Rognon (1990), Submicron desert dusts: A sandblasting process, *J. Geophys. Res.*, *95*, 13,927–13,935.

Goudie, A. S., I. Livingstone, and S. Stokes (Eds.) (1999), *Aeolian Environments, Sediments and Landforms*, John Wiley, Hoboken, N. J.

Huffman, G. J., et al. (1997), The Global Precipitation Climatology Project (GPCP) combined precipitation dataset, *Bull. Am. Meteorol. Soc.*, *78*, 5–20.

Kalnay, E. (1996), The NCEP/NCAR 40-year reanalysis project, *Bull. Am. Meteorol. Soc.*, *77*, 437–471.

Lima, J. L. D., P. M. Van Dijck, and W. P. Spaan (1992), Splash-saltation transport under wind-driven rain, *Soil Technol.*, *5*, 151–166.

Mahowald, N. M., and J.-L. Dufresne (2004), Sensitivity of TOMS aerosol index to boundary layer height: Implications for detection of mineral aerosol sources, *Geophys. Res. Lett.*, *31*, L03103, doi:10.1029/2003GL018865.

Mahowald, N. M., R. G. Bryant, J. del Corral, and L. Steinberger (2003a), Ephemeral lakes and desert dust sources, *Geophys. Res. Lett.*, *30*(2), 1074, doi:10.1029/2002GL016041.

Mahowald, N. M., C. Luo, J. del Corral, and C. S. Zender (2003b), Interannual variability in atmospheric mineral aerosols from a 22-year model simulation and observational data, *J. Geophys. Res.*, *108*(D12), 4352, doi:10.1029/2002JD002821.

McTainsh, G. H., J. F. Leys, and W. G. Nickling (1999), Wind erodibility of arid lands in the Channel Country of western Queensland, Australia, *Z. Geomorphol.*, *116*, 113–130.

McTainsh, G. H., B. M. Love, J. F. Leys, and C. Strong (2002), Wind erodibility of arid lands in the Channel Country of western Queensland, Australia: A sequel (1994–2000), paper presented at ICAR5/GCTE-SEN Joint Conference, U. S. Dep. of Agric., Lubbock, Tex.

Nicholson, S. E., C. J. Tucker, and M. B. Ba (1998), Desertification, drought, and surface vegetation: An example from the West African Sahel, *Bull. Am. Meteorol. Soc.*, *79*, 815–829.

Okin, G. S., D. A. Roberts, B. Murray, and W. J. Okin (2001), Practical limits on hyperspectral vegetation discrimination in arid and semiarid environments, *Remote Sens. Environ.*, *77*, 212–225.

Peters, A. J., and M. D. Eve (1995), Satellite monitoring of desert plant community response to moisture availability, *Environ. Monit. Assess.*, *37*, 273–287.

Prospero, J. M., and P. J. Lamb (2003), African droughts and dust transport to the Caribbean: Climate change implications, *Science*, *302*, 1024–1027.

Prospero, J. M., and R. T. Nees (1986), Impact of the North African drought and El Niño on mineral dust in the Barbados trade winds, *Nature*, *320*, 735–738, doi:10.1038/320735a0.

Prospero, J. M., P. Ginoux, O. Torres, S. E. Nicholson, and T. E. Gill (2002), Environmental characterization of global sources of atmospheric soil dust derived from the NIMBUS7 TOMS absorbing aerosol product, *Rev. Geophys.*, *40*(1), 1002, doi:10.1029/2000RG000095.

Pye, K. (1987), *Aeolian Dust and Dust Deposits*, Elsevier, New York.

Tegen, I., P. Hollrig, M. Chin, I. Fung, D. Jacob, and J. Penner (1997), Contribution of different aerosol species to the global aerosol extinction optical thickness: Estimates from model results, *J. Geophys. Res.*, *102*, 23,895–23,915.

Tegen, I., S. P. Harrison, K. E. Kohfeld, I. C. Prentice, M. T. Coe, and M. Heimann (2002), Impact of vegetation and preferential source areas on global dust aerosol: Results from a model study, *J. Geophys. Res.*, *107*(D21), 4576, doi:10.1029/2001JD000963.

Torres, O., P. K. Bhartia, J. R. Herman, A. Sinyuk, P. Ginoux, and B. Holben (2002), A long-term record of aerosol optical depth from TOMS observations and comparison to AERONET measurements, *J. Atmos. Sci.*, *59*, 398–413.

Washington, R., M. Todd, N. J. Middleton, and A. S. Goudie (2003), Dust-storm source areas determined by the Total Ozone Monitoring Spectrometer and surface observations, *Ann. Assoc. Am. Geogr.*, *93*, 297–313.

Weiss, J. L., D. S. Gutzler, J. E. A. Coonrod, and C. N. Dahm (2004), Seasonal and inter-annual relationships between vegetation and climate in central New Mexico, USA, *J. Arid Environ.*, *57*, 507–534.

Wurzler, S., T. G. Reisin, and Z. Levin (2000), Modification of mineral dust particles by cloud processing and subsequent effects on drop size distributions, *J. Geophys. Res.*, *105*, 4501–4512.

Zender, C. S., H. Bian, and D. Newman (2003a), Mineral Dust Entrainment And Deposition (DEAD) model: Description and 1990s dust climatology, *J. Geophys. Res.*, *108*(D14), 4416, doi:10.1029/2002JD002775.

Zender, C. S., D. J. Newman, and O. Torres (2003b), Spatial heterogeneity in aeolian erodibility: Uniform, topographic, geomorphic, and hydrologic hypotheses, *J. Geophys. Res.*, *108*(D17), 4543, doi:10.1029/2002JD003039.

E. Y. Kwon and C. S. Zender, Department of Earth System Science, University of California, Irvine, CA 92697-3100, USA. (zender@uci.edu)